Available online at www.sciencedirect.com
SCIENCE DIRECT®
Bioorganic & Medicinal Chemistry 12 (2004) 4147–4157
Bioorganic & Medicinal Chemistry

Inhibitory mode of indole-2-carboxamide derivatives against HLGPa: molecular docking and 3D-QSAR analyses ☆

Guixia Liu, Zhenshan Zhang, Xiaomin Luo,* Jianhua Shen, Hong Liu, Xu Shen, Kaixian Chen and Hualiang Jiang*

Drug Discovery and Design Center, State Key Laboratory of Drug Research, Shanghai Institute of Materia Medica, Shanghai Institutes for Biological Sciences, Chinese Academy of Sciences, 555 Zu Chong Zhi Road, Shanghai 201203, China

Received 7 April 2004; revised 17 May 2004; accepted 17 May 2004
Available online 17 June 2004

Abstract—The interaction of a series of indole-2-carboxamide compounds with human liver glycogen phosphorylase a (HLGPa) have been studied employing molecular docking and 3D-QSAR approaches. The Lamarckian Genetic Algorithm (LGA) of AutoDock 3.0 was employed to locate the binding orientations and conformations of the inhibitors interacting with HLGPa. The binding models were demonstrated in the aspects of inhibitor's conformation, subsite interaction, and hydrogen bonding. The very similar binding conformations of these inhibitors show that they interact with HLGPa in a very similar way. Good correlations between the calculated interaction free energies and experimental inhibitory activities suggest that the binding conformations of these inhibitors are reasonable. The structural and energetic differences in inhibitory potencies of indole-2-carboxamide compounds were reasonably explored. Using the binding conformations of indole-2-carboxamides, consistent and highly predictive 3D-QSAR models were developed by CoMFA and CoMSIA analyses. The q^2 values are 0.697 and 0.622 for CoMFA and CoMSIA models, respectively. The predictive ability of these models was validated by four compounds that were not included in the training set. Mapping these models back to the topology of the active site of HLGPa leads to a better understanding of the vital indole-2-carboxamide–HLGPa interactions. Structure-based investigations and the final 3D-QSAR results provide clear guidelines and accurate activity predictions for novel inhibitor design.

1. Introduction

Diabetes mellitus, the most common hormonal deficiency disease, is characterized by chronic elevated blood glucose levels. There are two forms of diabetes, that is type 1 diabetes and type 2 diabetes. For type 1 diabetes, the autoimmune-mediated destruction of pancreatic β-cell islets results in absolute insulin deficiency. Type 2 diabetes mellitus, which accounts for 90–95% of cases, is characterized by peripheral insulin resistance and pancreatic defects in insulin secretion, although the metabolic basis of the disease has not well understood.[1–3] Type 2 diabetes usually leads to complications such as nerve and kidney damage, blindness, premature atherosclerosis, and heart disease.[4] Indeed, it is now generally accepted that those late complications are the direct result of a chronically elevated blood glucose level. At present, therapy for type 2 diabetes relies on diet, exercise, and hypoglycemic drugs intended to reduce the hyperglycaemia. Unfortunately, tight control of plasma glucose is generally impossible with current oral hypoglycemic agents. Moreover, their chronic use often brings, in addition to toleration, fear of dangerous hypoglycemic episodes.[5] Safer and more effective therapy is urgently needed.

The liver is the predominant source of plasma glucose in fasting type 2 diabetics.[6–9] The liver produces glucose by two pathways, gluconeogenesis (de novo synthesis of glucose) and glycogenolysis (break-down of glycogen by phosphorylase). A reported data, showing that much of glucose arising from gluconeogenesis has cycled through glycogen,[10] expose a possibility that inhibition of glycogen phosphorylase (GP) could suppress hepatic glucose arising from both pathways.[11] Furthermore, a number of experimental and theoretical studies[11–32] have

Keywords: Indole-2-carboxamide inhibitors; HLGPa; Docking; 3D-QSAR; CoMFA; CoMSIA.
☆ Supplementary data associated with this article can be found, in the online version, at doi:10.1016/j.bmc.2004.05.023
* Corresponding authors. Tel.: +86-21-50807188; fax: +86-21-50807088; e-mail: hljiang@mail.shcnc.ac.cn

0968-0896/$ - see front matter © 2004 Elsevier Ltd. All rights reserved.
doi:10.1016/j.bmc.2004.05.023

been performed on GP since human liver GPa (HLGPa) was believed to be an important target enzyme in terms of the treatment of type 2 diabetes because of its direct influence on blood sugar level. Most reported phosphorylase inhibitors are glucose or other sugar-based analogues,[12–21] which have in numerous instances been shown to bind at the catalytic site of GP. Recently, much attention has been paid to the indole-2-carboxamide analogs, which bind at the novel allosteric site of HLGPa.[11,29–31] These inhibitors inhibit the enzyme activity synergistically with glucose. The synergism could be an important physiological feature of a GP inhibitor, because the decrease in inhibitory potency, as glucose concentrations decrease in vivo, should minimize the risk of hypoglycaemia. Hoover et al. designed and synthesized a series of indole-2-carboxamide analogs[29] derived from compound **1** (Cp91149) (Table 1(Panels A and B)). Among them, compound **14** is the most active.

To the best of our knowledge, no previous effort has been carried out to seek new insight into the relationship between the structure information with the inhibitory potency of indole-2-carboxamides employing combined computational methods of automated molecular docking with 3D-QSAR approaches. In this paper, we studied the binding mode of indole-2-carboxamide derivatives[29] against HLGPa using automated molecu-

Table 1. Structures and in vitro phosphorylase inhibitory activity of 3-[(indole-2-carbonyl)amino]-2-hydroxy-4-phenylbutyric acid analogues (Panel A) and *N*-(indole-2-carbonyl) phenylalanine analogues (Panel B)

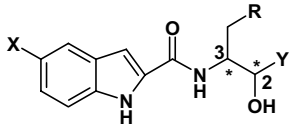

Compd	X	R	Y	*	IC_{50} (nM)	$-\log IC_{50}$	ΔG (kcal/mol)
Panel A							
1	Cl	Ph	$CONMe_2$	3*S*,2*R*	110 ± 2	6.96 ± 0.05	−11.98
2	Cl	Ph	$CONMe_2$	3*R*,2*S*	1800 ± 320	5.74 ± 0.07	−10.35
3	Cl	Ph	$CONMe_2$	3*R*,2*R*	1700 ± 190	5.77 ± 0.05	−11.08
4	Cl	Ph	$CONMe_2$	3*S*,2*S*	8700 ± 1700	5.06 ± 0.08	−9.43
5	F	Ph	$CONMe_2$	3*S*,2*R*	170 ± 16	6.77 ± 0.04	−11.32
6	Br	Ph	$CONMe_2$	3*S*,2*R*	97 ± 11	7.01 ± 0.04	−12.32
7	H	Ph	$CONMe_2$	3*S*,2*R*	440 ± 48	6.36 ± 0.05	−11.09
8	Cl	Ph	CONHMe	3*S*,2*R*	680 ± 37	6.17 ± 0.03	−11.74
9	Cl	Ph	$CONH_2$	3*S*,2*R*	1700 ± 140	5.77 ± 0.03	−10.97
10	Cl	Ph	COOH	3*S*,2*R*	330 ± 31	6.48 ± 0.04	−11.11
11	Cl	Cy[a]	$CONMe_2$	3*S*,2*R*	6500 ± 610	5.19 ± 0.04	−9.59
12*	Cl	Ph	COOMe	3*S*,2*R*	210 ± 40	6.68 ± 0.08	−12.26
13*	Cl	Ph	CH_2OH	3*S*,2*R*	6800 ± 1700	5.17 ± 0.10	−9.76
Panel B							

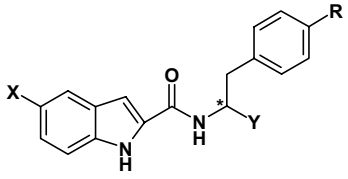

14	Cl	H	$CONMe_2$	*S*	82 ± 10	7.09 ± 0.05	−12.72
15	Cl	H	CONHMe	*S*	110 ± 10	6.96 ± 0.04	−11.70
16	Br	H	$CONMe_2$	*S*	110 ± 8	6.96 ± 0.03	−11.82
17	F	H	$CONMe_2$	*S*	430 ± 44	6.37 ± 0.05	−10.54
18	H	H	$CONMe_2$	*S*	400 ± 45	6.40 ± 0.05	−10.61
19	OMe	H	$CONMe_2$	*S*	4700 ± 300	5.33 ± 0.03	−9.90
20	Cl	H	CO (1-piperidin-4-ol)	*S*	260 ± 17	6.59 ± 0.03	−12.46
21	Cl	F	CO (1-piperidin-4-ol)	*S*	205 ± 16	6.69 ± 0.03	−13.03
22	Cl	H	COOMe	*S*	140 ± 18	6.85 ± 0.05	−12.07
23	Cl	H	COOH	*S*	1700 ± 490	5.77 ± 0.11	−11.01
24*	Cl	H	$CONMe_2$	*R*	260 ± 33	6.59 ± 0.06	−10.46
25*	Cl	H	CONHMe	*R*	220 ± 32	6.66 ± 0.06	−11.12

* Compounds that were not included in the construction of 3D-QSAR models.
[a] Cyclohexyl.

lar docking approach. Following the docking results, 3D-QSAR models were constructed by using approaches of comparative molecular field analysis (CoMFA)[33] and comparative molecular similarity analysis (CoMSIA).[34] The aims of the present research include three aspects. The first one is to demonstrate the common binding mode of indole-2-carboxamide inhibitors with HLGPa. The second one is to predict the binding free energy relative to the inhibitory potency of these compounds. The last, but the most important, is to obtain QSAR models involving the main intermolecular interactions between inhibitors and HLGPa, which can not only be used in rapidly and accurately predicting the activities of new designed inhibitors, but also offer some beneficial clues in structural modifications for designing new inhibitors with much higher inhibitory activities against HLGPa.

2. Computational details

The crystal structure of HLGPa in complex with its inhibitor Cp403700 (PDB entry 1EXV)[30] was applied in this research, because there was no crystal structure of HLGPa in complex with inhibitor **1** (Cp91149, Table 1(Panel A)), and the crystal structure of HLGPa complexed with compound **23** (Cp320626) is not suitable for this system due to its monomer structure. The molecular modeling software Sybyl 6.8[35] was employed for CoMFA[33] and CoMSIA[34] analyses and visualization. All calculations were performed on SGI Origin 3200 server.

2.1. Molecular docking

The crystal structure of HLGPa in complex with its inhibitor Cp403700 (PDB entry code 1EXV) was recovered from Brookhaven Protein Database (PDB http://www.rcsb.org/pdb). The potential of the 3D structures of HLGPa was assigned according to the Amber 4.0 force field with Kollman-united-atom[36] charges encoded in Sybyl 6.8.[35] The initial structures of 25 compounds (Table 1(Panels A and B)) were constructed based on the structure of inhibitor Cp403700 (Fig. 1) by Sybyl 6.8.[35] The geometries of these compounds were subsequently optimized using the MMFF94 force field,[37] MMFF94 charges,[37] and Powell method; a nonbond cutoff of 8 Å[38–40] was adopted to consider the intramolecular interaction.

For the purpose of tackling the interacting mode of indole-2-carboxamides (inhibitors) with HLGPa (enzyme), the advanced docking program AutoDock 3.0.3[41,42] was used to perform the automated molecular docking. The Lamarckian genetic algorithm (LGA)[42] was applied to deal with the inhibitor–enzyme interactions. Briefly, the LGA described the relationship between the inhibitors and the enzymes by the translation, orientation, and conformation of the inhibitors. These so-called 'state variables' were the inhibitors' genotype,

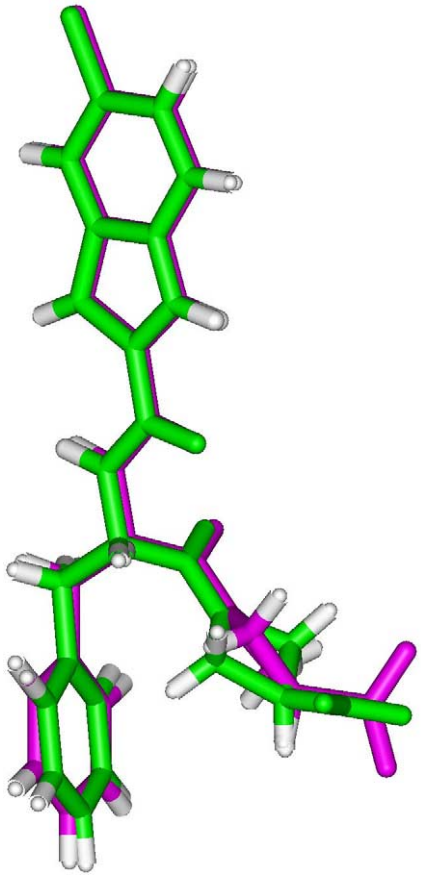

Figure 1. Conformational comparison of Cp403700 from the crystal structure (green) and that from the AutoDock result (magenta).

and the resulting atomic coordinates together with the interaction and the intramolecular energies were the inhibitors' phenotype. The environmental adaptation of the phenotype was reverse-transcribed into its genotype and became heritable traits. Each docking cycle, or generation, consisted of a regimen of fitness evaluation, cross-over, mutation, and selection. A Solis and Wets local search[43] performed the energy minimization on a user-specified proportion of the population. The docked structures of the inhibitors were generated after a reasonable number of evaluations. The whole docking operation could be stated as follows.

First, the HLGPa molecule was checked for polar hydrogens and assigned for partial atomic charges, the PDBQs file was created, and the atomic solvation parameters were also assigned for the macromolecules.

Second, the 3D grid with $60\times60\times80$ points and a spacing of 0.375 Å was created by the AutoGrid algorithm[42] to evaluate the binding energies between the inhibitors and the HLGPa. In this stage, the HLGPa was embedded in the 3D grid and a probe atom was placed at each grid point. The affinity and electrostatic potential grid were calculated for each type of atom in the inhibitors. The energetics of a particular inhibitor configuration was found by trilinear interpolation of affinity values and electrostatic interaction of the eight

grid points surrounding each of the atoms in an inhibitor.

Third, a series of the docking parameters were set on. Not only the atom types but also the generations and the number of runs for the LGA algorithm were edited and properly assigned according to the requirement of the Amber force field. The number of generations, energy evaluations, and docking runs were set to 27,000, 1,500,000, and 20, respectively. The kinds of atomic charges were taken as Kollman-united-atom[36] for HLGPa and MMFF94[37] for the inhibitors.

Finally, the docked complexes of inhibitor–enzyme were selected according to the criteria of interacting energy combined with geometrical matching quality. These complexes were used as the starting conformation for further energetic minimization and geometrical optimization before the final models were achieved.

2.2. Binding free energy prediction

Typically, three binding energy terms used in the previous versions of AutoDock[44] were included in the score function: the van der Waals interaction represented as a Lennard-Jones 12–6 dispersion/repulsion term, the hydrogen bonding represented as a directional 12–10 term, and the Coulombic electrostatic potential. So, the binding energy of indole-2-carboxamide compounds with HLGPa could be simply described as the electrostatic, van der Waals, and hydrogen-bonding interaction energy, respectively.

On the basis of the traditional molecular force field model of interaction energy, a new score function at the level of binding free energy was derived and adopted in the version of AutoDock 3.0.3.[41,42] Not only the restriction of internal rotors, the global rotation, and the translation were modeled depending on the number of torsion angles of the ligand but also the desolvation upon binding and the hydrophobic effect (solvent entropy changes at solute-solvent interfaces) were calculated. The total binding free energy was empirically calibrated based on the above-stated terms and a set of coefficient factors.[42] Thus, the new score function was sufficient to rank the inhibitors in the different levels of binding affinities. The same rationale was applied to the system of indole-2-carboxamide compounds and HLGPa in order to evaluate the binding properties more precisely than the traditional molecular mechanics method did, and the total binding free energy between indole-2-carboxamides and HLGPa was calculated using the algorithm in the AutoDock 3.0.3 program.[41,42]

2.3. 3D-QSAR analyses

To more fully explore the specific contributions of electrostatic, steric, and hydrophobic effects in the binding of indole-2-carboxamides to HLGPa and to build predictive QSAR models, CoMFA[33] and CoMSIA[34] studies were performed for these inhibitors based on the conformational alignments predicted from the molecular docking.

2.3.1. CoMFA. Usually, steric and electronic field energies were probed using an sp^3 carbon atom and a +1 net charge atom, respectively. Steric and electrostatic interactions were calculated using the Tripos force field[45] with a distance-dependent dielectric constant at all intersections in a regularly spaced (2 Å) grid. The minimum σ (column filtering) was set to 2.0 kcal/mol to improve the signal-to-noise ratio by omitting those lattice points whose energy variation was below this threshold. A cutoff of 30 kcal/mol was adopted, and the regression analysis was carried out using the full cross-validated partial least-squares (PLS) method (leave one out) with CoMFA standard options for scaling of variables. The final model (noncross-validated conventional analysis) was developed with the optimum number of components equal to that yielding the highest q^2.

2.3.2. CoMSIA. For the CoMSIA calculation, three physicochemical properties, namely steric, electrostatic, and hydrophobic fields, have been evaluated. The steric contribution was reflected by the third power of the atomic radii of the atoms. Electrostatic properties were introduced as atomic charges resulted from molecular docking. An atom-based hydrophobicity was assigned according to the parametrization developed by Ghose et al.[46] The lattice dimensions were selected with a sufficiently large margin (>4 Å) to enclose all aligned molecules. Singularities were avoided at atomic positions in CoMSIA fields because a Gaussian type distance dependence of the physicochemical properties was adopted, thus no arbitrary cutoffs were required. In general, similarity indices, $A_{F,K}$, between the compounds of interest were computed by placing a probe atom at the intersections of the lattice points using Eq. 1,

$$A_{F,K^q}(j) = -\sum_{i=1}^{n} W_{probe,k} W_{ik}\, e^{-a r_{iq}^2} \qquad (1)$$

where q represents a grid point; i is the summation index over all atoms of the molecule j under computation; W_{ik} is the actual value of the physicochemical property k of atom i; and $W_{probe,k}$ is the value of the probe atom. In the present study, similarity indices were computed using a probe atom ($W_{probe,k}$) with charge +1, radius 1 Å, hydrophobicity +1, and attenuation factor α of 0.3 for the Gaussian type distance. The statistical evaluation for the CoMSIA analyses was performed in the same way as described for CoMFA.

3. Results and discussion

3.1. Interactions between inhibitors and HLGPa

3.1.1. Inhibitor's conformation. The automated molecular docking may produce several options of binding conformation for each inhibitor. The conformation

corresponding to the lowest binding energy with HLGPa was selected as the possible binding conformation. The conformational superposition of Cp403700 from the X-ray crystal structure and that from the AutoDock result is shown in Figure 1. The root mean square deviation (RMSD) between these two conformation is ~0.50 Å, indicating that the parameter set for the AutoDock simulation is reasonable to reproduce the X-ray structure. The AutoDock method and the parameter set could be extended to search the binding conformations of other inhibitors accordingly. Figure 2A represented the 3D model of inhibitor–HLGPa complexes, and Figure 2B demonstrates the probable binding conformational alignment for these indole-2-carboxamide inhibitors extracted from the AutoDock inhibitor–HLGPa complexes. Just like Cp403700 co-crystallized with HLGPa, indole-2-carboxamides locate in the region of the central cavity, at the subunit interface, and share some common binding features for each other. All of the indole-2-carboxamides are bound in the novel allosteric site of HLGPa in a similar conformation of Cp403700 in the X-ray structure cocrystallized with HLGPa (Fig. 2), and the binding conformations of indole-2-carboxamides could be aligned fairly well overall.

3.1.2. Interactions of subsites. To illustrate the interaction mechanism, inhibitor **14**, the most potent inhibitor among the 25 indole-2-carboxamides, was selected for more detailed analysis. In the latter discussions, all the descriptions referred to the inhibitor **14** unless otherwise noted. Figure 3A generally represents the interacting model of inhibitor **14** with HLGPa. In general, the indole-2-carboxamides can be separated into the indole and carboxamide moieties. While the latter can be considered in detail to comprise three parts, namely, the acidamide, benzyl, and Y substituent.

The indole moieties of all the 21 indole-2-carboxamide compounds of the training set locate much at the same site (Fig. 2). It can be seen from Figure 3A that the chloroindole moiety of compound **14** is surrounded by residues Val40′, Arg60, Val64, Trp67, Trp189, and Lys191 mainly through the hydrophobic interaction. In addition, the indole nitrogen forms a hydrogen bond to the backbone carbonyl of Glu190, and the guanidinium group of Arg60 appears to have a favorable electrostatic interaction with the indole ring. The plane composed by the heavy atoms of the guanidinium group of Arg60 is almost parallel to the indole ring. There is weak steric restriction in the vicinity of X substituent, so the bromine, chlorine, and fluorin substituents provide superior inhibitory potencies over hydrogen atom. This plus the electrostatic interaction with Arg60 is the reason why the inhibitory activities of compounds have the order of $\mathbf{6 > 1 > 5 > 7}$. And the similar inhibitory activity in the order of $\mathbf{16 \approx 14 > 17 \approx 18}$ is also due to the same reasons.

Compared with the indole ring, the carboxamide moiety seems much more flexible. The carboxamide moiety is both hydrophobic and polar. In the acidamide portion, there is only one hydrogen bond between the amide nitrogen next to the indole ring and Thr38′. The Y substituent, most of which is exposed to the solvent, forms a hydrophobic interaction contact with the side chain of Ser192 and a hydrogen bond with Lys191. Because of the hydrophobic interaction, the more

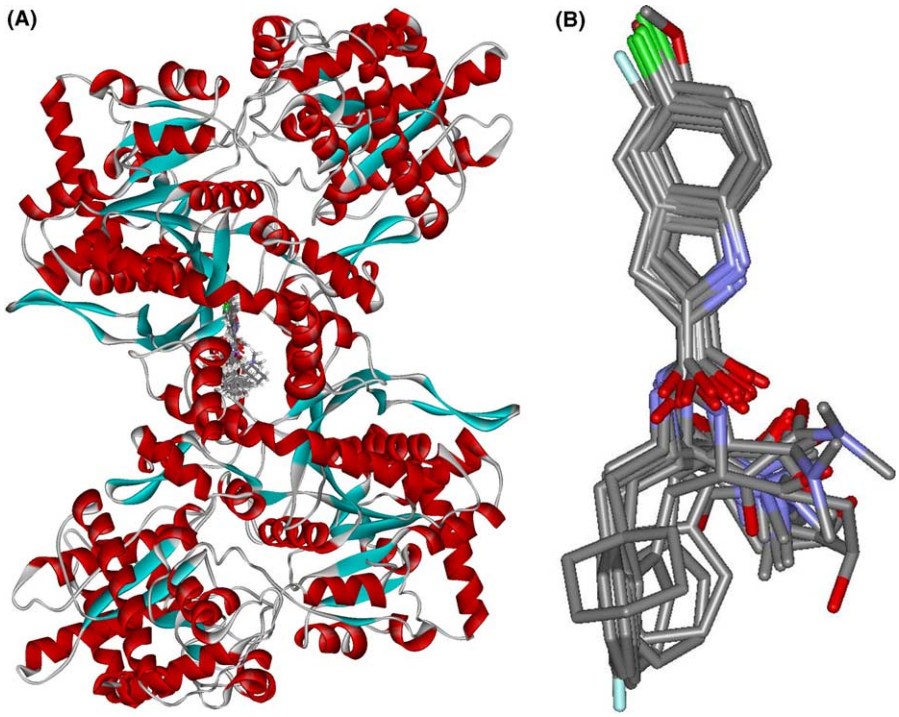

Figure 2. (A) The three-dimensional structural model of indole-2-carboxamide inhibitors–HLGPa complex. (B) Probable binding conformations of indole-2-carboxamide analogues and their alignment in the novel allosteric site of HLGPa.

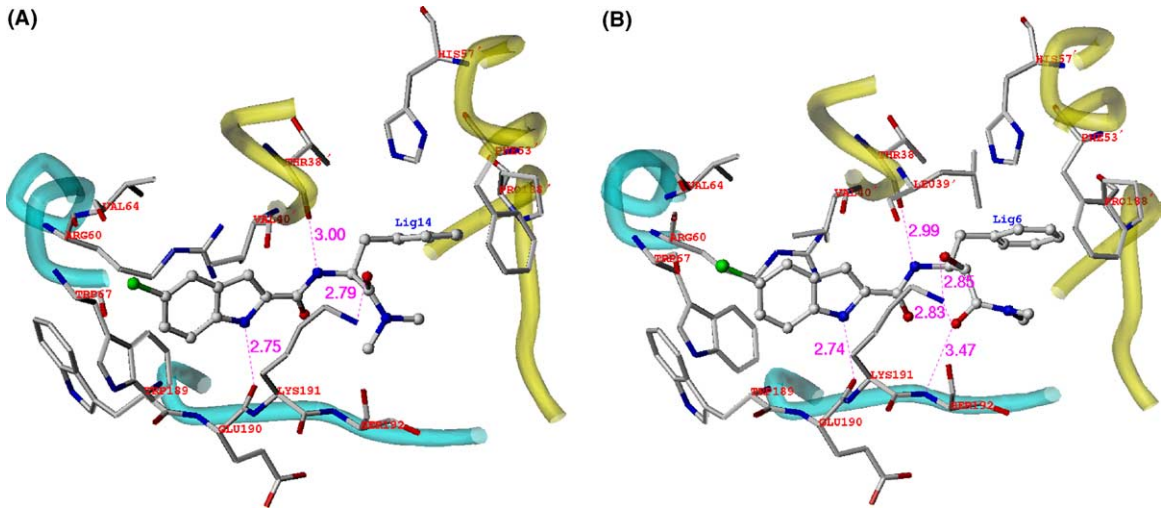

Figure 3. The interacting modes of compounds **14** (A) and **6** (B) with HLGPa. The inhibitors and the important residues for inhibitor–protein interaction are represented by ball-and-stick and stick models, respectively. The magenta dashed lines denote the hydrogen bonds.

hydrophobic substituent in Y moiety may lead to more inhibitory activity. This may rationalize why the inhibitory activity of compounds have the order of **1** > **8** > **9** and **14** > **16**. As for the benzyl segment, it is obvious that the phenyl group binds the side chains of Phe53′, His57′, and Pro188′ through the hydrophobic interaction.

3.1.3. Hydrogen-bonding interactions. Following a similar binding pattern, hydrogen bonding is one important characteristic of the interaction between the indole-2-carboxamides and the HLGPa. There are mainly three hydrogen bonds formed between the indole-2-carboxamides and some residues in HLGPa. It can be seen clearly from Figure 3A that the indole nitrogen of compound **14** acts as a donor to form a hydrogen bond with the backbone carbonyl of Glu190. Similarly, as a hydrogen donor, the amide nitrogen next to the indole moiety also forms a hydrogen bond with the backbone carbonyl of Thr38′. The third hydrogen bond is formed between the carbonyl in Y moiety of compound **14** as an acceptor and the N^{ζ} atom of the Lys191 side chain. The hydrogen-bonding acts as an 'anchor', intensely determining the 3D space position of the indole ring and the Y moiety in the binding pocket and facilitating the hydrophobic interaction of the aromatic and heterocyclic rings with the side chain of Val40′, Phe53′, His57′, Arg60, Val64, Trp67, Pro188′, Trp189, and Ser192.

The compounds (**1**–**13***) in Table 1(Panel A), which have a CHOH group more than those in Table 1(Panel B), form additional hydrogen bonds with the residues of HLGPa besides the three main hydrogen bonds described above. To illuminate visually, the interacting model of compound **6** (a compound in Table 1(Panel A)) with HLGPa was represented in Figure 3B. It is the excessive CHOH group close to the Y moiety that leads to the additional hydrogen bonds. Either the hydroxyl of CHOH group forms a hydrogen bond with the N^{ζ} atom of Lys191 as an acceptor or it interacts with the backbone carbonyl of Thr38′ as a donor (see Fig. 3B). In addition, a weak hydrogen bond may forms between the carbonyl of Y moiety and N atom of the backbone of Ser192.

3.2. The correlation between binding free energy and inhibitory activity

The predicted binding free energies of the indole-2-carboxamides binding to HLGPa are also listed in Table 1(Panels A and B). Satisfied that the 3D structures of indole-2-carboxamides–HLGPa complexes were indeed reasonable, we then performed a linear regression analysis to explore whether the inhibitory potencies of the indole-2-carboxamide inhibitors could be correlated with the energetic parameters. By using experimentally determined IC_{50} values, we calculated the regression equation for the inhibitory activities, $-\log IC_{50}$ values, using the total binding free energies, ΔG, as the sole descriptor variable. A good correlation was found between the inhibitory activities and the predicted binding energies (Eq. 2), and this relationship is graphically shown in Figure 4. The relationship suggests that those potential HLGPa inhibitors exhibiting stronger binding free energies using this paradigm would, therefore, be expected to have greater efficacy toward inhibitory action. This good correlation further demonstrates the reasonability of the binding conformations and binding models for the indole-2-carboxamide inhibitors with HLGPa.

$$-\log IC_{50} = 0.197 - 0.541 \times \Delta G \quad (n = 21,\ r^2 = 0.710,\ F = 46.578,\ s = 0.352) \qquad (2)$$

Based on the binding free energies and their correlation with the inhibitory activities, we can give a more quantitative explanation to the structure–activity relationship of the inhibitory mechanism for these inhibitors. It is obvious that there would be about a 1.8 kcal/mol difference in binding free energy if there is one order

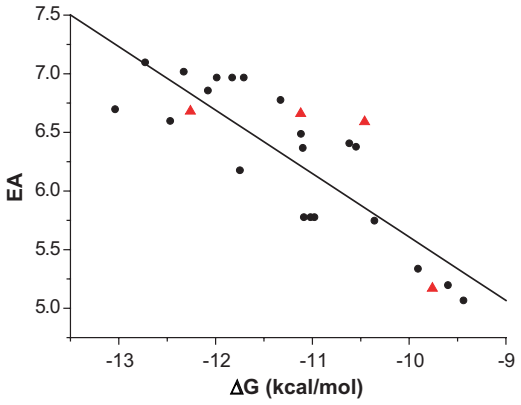

Figure 4. Correction between the binding free energy (ΔG, kcal/mol, $T = 298.15$ K) of indole-2-carboxamide compounds with HLGPa and the experimental activities ($-\log IC_{50}$, EA). ●, compounds of the training set; ▲, compounds of the testing set.

of magnitude for numerical difference in the inhibitory potency (IC_{50}). For example, the increased absolute values in the binding free energies of compounds **5**, **1**, and **6** as compared with compound **7** are 0.23, 0.89, and 1.23 kcal/mols, respectively. These increases of the absolute values in the binding free energies, caused by the substitution of F, Cl, and Br for H, can attribute to both the favorable steric interaction and the enhancement of the electrostatic interaction of the indole 5-substituent with guanidinium group of Arg60.

AutoDock scoring function is expressed as a sum of van der Waals, electrostatic, hydrogen bonding, loss of entropic term (torsional freedom), and desolvation terms. The binding free energy of the inhibitors and protein can be, in general, decomposed as electrostatic and nonelectrostatic parts (Table S1 in the Supporting information). It can be estimated that the average electrostatic contribution to the inhibitor–HLGPa binding is about 6.1%, indicating that the nonelectrostatic interaction dominates the binding of inhibitors to HLGPa. This is in agreement with the structural properties of the binding pocket of HLGPa, which is much hydrophobic.[30]

3.3. 3D-QSAR models

3.3.1. CoMFA. Although CoMFA is not able to appropriately describe all of the binding force, being based principally on standard steric and electrostatic molecular fields to model substrate–enzyme interactions, it is still a widely used tool for the study of QSAR at the 3D level. The major objective of CoMFA analysis for the indole-2-carboxamides is to find the best predictive model within the system. We picked up 21 indole-2-carboxamide inhibitors for CoMFA analyses, the other four as testing compounds for the model validations. PLS analysis results based on least-squares fitting are listed in Table 2, which shows that all of the statistical indexes are reasonably high. The predicted activities (PA) of the 21 indole-2-carboxamide inhibitors from the 3D-QSAR model versus their inhibitory activities (EA) are compiled in Table 3, and the correlation between PA and EA is presented in Figure 5A. As listed in Table 2, a CoMFA model with a cross-validated q^2 of 0.697 for six components was obtained based on the binding conformations and their alignment in the active site of HLGPa. The noncross-validated PLS analysis was performed with the optimum components of six, as determined by the cross-validated analysis, to give a conventional r^2 of 0.996, $F = 662.217$, and the estimated standard error of 0.045. These values indicated a good conventional statistical correlation as shown in Figure 5A, and a satisfactory predictive ability of the CoMFA model.

3.3.2. CoMSIA. CoMSIA analysis results are also summarized in Table 2. A CoMSIA model with a cross-validated q^2 of 0.622 for four components and a conventional r^2 of 0.965 was obtained. These data demonstrate that the CoMSIA model is also fairly predictive. The predicted inhibitory potencies of indole-2-carboxamides against HLGPa are listed in Table 3 and their correlation is shown in Figure 5B. The high value of the conventional r^2 relating to five different descriptor variables (steric, electrostatic, hydrophobic, hydrogen-bond donor and acceptor) illustrates that these variables are necessary to describe the interaction mode of indole-2-carboxamide inhibitors with HLGPa, as well as the field properties around the inhibitors. The corresponding field distributions (Table 2) of these five descriptor variables are 9.0%, 24.2%, 17.8%, 19.2%, and 29.9%, respectively, which indicates that hydrogen bond interactions play a crucial role in locating the indole-2-carboxamide compounds in the novel allosteric site of HLGPa. The CoMSIA field distributions also indicate that the nonelectrostatic interaction dominates the binding between the inhibitors and HLGPa, which is

Table 2. Statistical indexes of CoMFA and CoMSIA models based on 21 indole-2-carboxamide compounds binding conformers

	Cross-validated		Conventional		
	q^2	Optimal comp.	r^2	s	F
CoMFA	0.697	6	0.996	0.045	662.217
CoMSIA	0.622	4	0.965	0.133	110.330
		Field distribution (%)			
Steric		51.8		9.0	
Electrostatic		48.2		24.2	
Hydrophobic				17.8	
H-bond donor				19.2	
H-bond acceptor				29.9	

Table 3. Predicted activities (PA) versus experimental activities (EA, $-\log IC_{50}$) and residues (δ) by CoMFA and CoMSIA

Compd	EA	CoMFA		CoMSIA	
		PA	δ	PA	δ
1	6.96	6.99	−0.03	6.88	0.08
2	5.74	5.74	0.00	5.96	−0.22
3	5.77	5.75	0.02	5.71	0.06
4	5.06	5.04	0.02	5.05	0.01
5	6.77	6.80	−0.03	6.82	−0.05
6	7.01	6.90	0.11	6.80	0.21
7	6.36	6.42	−0.06	6.48	−0.12
8	6.17	6.14	0.03	6.21	−0.04
9	5.77	5.77	−0.00	5.62	0.15
10	6.48	6.46	0.02	6.49	−0.01
11	5.19	5.25	−0.06	5.22	−0.03
12*	6.68	6.20	0.48	6.69	−0.01
13*	5.17	6.09	−0.92	6.06	−0.89
14	7.09	7.07	0.02	6.94	0.15
15	6.96	6.99	−0.03	6.80	0.16
16	6.96	6.96	−0.00	6.93	0.03
17	6.37	6.33	0.04	6.52	−0.15
18	6.40	6.40	−0.00	6.63	−0.23
19	5.33	5.30	0.03	5.23	0.10
20	6.59	6.58	0.01	6.60	−0.01
21	6.69	6.73	−0.04	6.73	−0.04
22	6.85	6.86	−0.01	6.90	−0.05
23	5.77	5.79	−0.02	5.77	−0.00
24*	6.59	5.76	0.83	5.66	0.93
25*	6.66	6.27	0.39	6.07	0.59

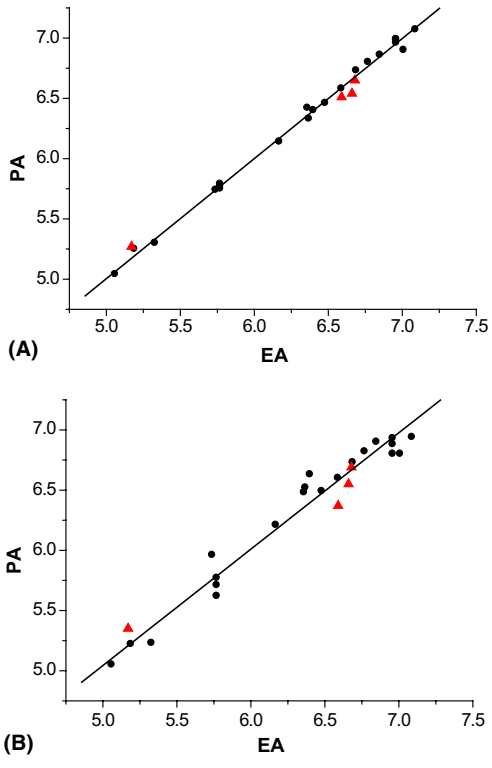

Figure 5. Predicted activities (PA) by CoMFA (A) and CoMSIA (B) models versus experimental activities (EA) of indole-2-carboxamides. ●, compounds of the training set; ▲, compounds of the testing set.

qualitatively in agreement with the binding free energy distribution (Table S1 in the Supporting information).

3.3.3. Validation of the 3D-QSAR models. To validate the stability and predictive ability of our 3D-QSAR model, four indole-2-carboxamide compounds (compounds **12***, **13***, **24***, and **25*** in Table 1) that were not included in the construction of CoMFA and CoMSIA models were selected as the testing compounds. The results are also listed in Table 3 (star labeled) and simultaneously displayed in Figure 5 (in black triangle (red in the web version)). It can be seen clearly from Figure 5 that the predicted $-\log IC_{50}$ (PA) values of the four testing compounds are in good agreement with the experimental data in a statistically tolerable error range, $r^2 = 0.996$ and 0.965 for CoMFA and CoMSIA models, respectively. The testing results for the four indole-2-carboxamide compounds indicate that the CoMFA and CoMSIA models can be further used in new indole-2-carboxamide inhibitors design for HLGPa.

3.4. CoMFA and CoMSIA contour maps correlate with HLGPa topology

The CoMFA map based on the alignments of the binding conformations is illustrated in Figure 6A. Compound **14** is displayed in the map in aid of visualization. Colored polyhedra in the map show these areas in 3D space where changes in the field values for indole-2-carboxamides correlate strongly with concomitant changes in inhibitory activities. Detrimental and beneficial steric interactions are, respectively, displayed in yellow and green contours, while blue and red contours illustrate the regions of desirable positive and negative electrostatic interactions. A large region of green contour around the R group suggests that more bulky substituents in these positions will significantly improve the biological activities. Since many bulky groups such as *tert*-butyl, cyclohexyl, and phenyl are hydrophobic, they may also be able to take advantage of the hydrophobic nature of the environment around Phe53′. The yellow polyhedron near the terminal of Y moiety indicates that increased steric bulk is unfavorable for the inhibitory activities. Adding more bulky groups around the yellow polyhedron may bring steric clash of these inhibitors with Lys191 and Ser192 of HLGPa, or the substituted bulky groups may be exposed to solvent; neither of these situations are beneficial to the inhibitor–HLGPa binding. The blue contours around the common chiral carbon of the inhibitors and the terminal of Y moiety suggest that positively charged substituents may increase the inhibitory activity. Two small red polyhedra located in the solvent-exposed resign of Y moiety indicate that high electron density may play a favorable role in inhibitory potencies.

The steric and electrostatic field distributions of CoMSIA, as shown in Figure 6B, are generally in accordance with the field distributions of CoMFA map (Fig. 6A). Furthermore, the hydrophobic analysis of CoMSIA, based on the hydrophobic distribution, could demonstrate more clearly the hydrophobic interactions between the indole-2-carboxamide derivatives and HLGPa. In the hydrophobic maps of CoMSIA (Fig. 6C), the yellow and white polyhedra represent the

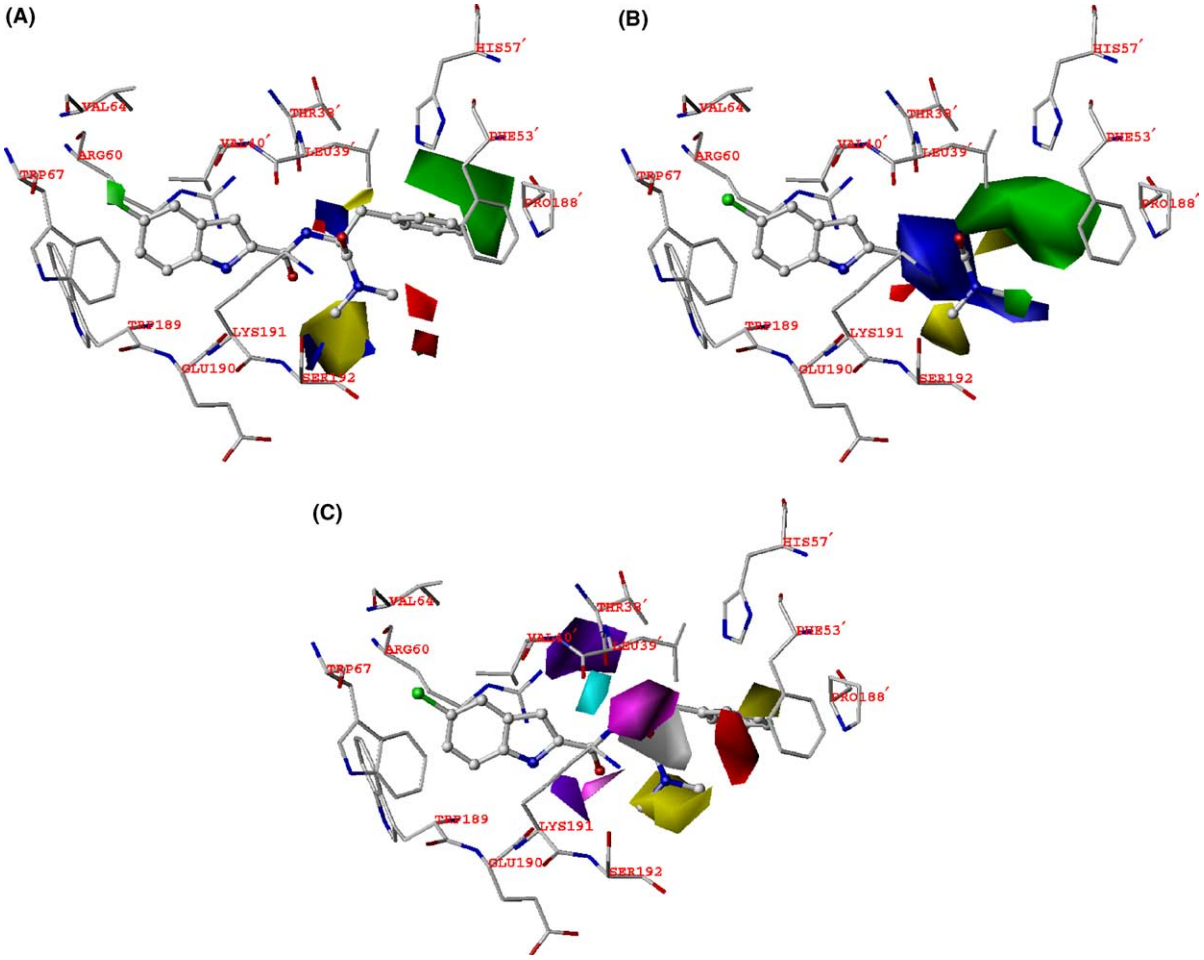

Figure 6. Contour maps as compared with the topology of **14**–HLGPa complex. Only residues relevant to the discussion are shown for clarity. (A) CoMFA; (B) the steric and electrostatic field distributions of CoMSIA; (C) the hydrophobic, H-bond donor and acceptor field distributions of CoMSIA. The residues are represented as sticks, and the inhibitor is shown in ball-and-stick. Sterically favored areas are in green; sterically unfavored areas are in yellow. Positive-charge-favored areas are in blue; positive-charge-unfavored areas are in red. Hydrophobic favored areas are in yellow; hydrophilic favored areas are in white. H-bond-donor-favored areas are in cyan; H-bond-donor-unfavored areas are in purple. H-bond-acceptor-favored areas are in magenta; H-bond-acceptor-unfavored areas are in red.

regions of favorable and unfavorable hydrophobic interactions, respectively. As shown in Figure 6C, one large yellow contour around R group shows that this structural moiety interacts with the side chains of residues at the binding site of HLGPa through hydrophobic interaction. This interaction model coincides with the hydrophobic property of the side chains of the residues around this part, especially obvious around Phe53′. The other yellow contour near the left part of the end of Y moiety illustrates that more hydrophobic substituents will increase the inhibitory activity of the indole-2-carboxamide compounds by forming hydrophobic interaction with the side chain of Lys191 and Ser192. The white contour around the carbonyl group of Y moiety of compound **14** suggests that more hydrophilic group substitutions will increase inhibitory potencies due to the hydrophilicity of the environmental residues Thr38′ and Lys191. For the hydrogen bond donor and acceptor maps of CoMSIA, as shown in Figure 6C, the cyan and magenta contours around the binding site indicate that hydrogen bond donors and acceptors are advantageous in these areas, respectively. This is in agreement with the inhibitor–protein binding model. As hydrogen bond acceptors, Lys191 and Ser192 form hydrogen bonds with indole-2-carboxamide compounds; while Thr38′ and Glu190 form hydrogen bonds with indole-2-carboxamide compounds as hydrogen bond donors. The consistency between the CoMSIA field distributions and the structural topological properties of the HLGPa binding site demonstrates the reasonability of the CoMSIA result.

The binding mode of indole-2-carboxamides with HLGPa, which was described in the interaction mechanism section, can also be readily observed from the CoMFA and CoMSIA maps by combing the CoMFA and CoMSIA contour maps with the 3D structural topology of the HLGPa binding site. Not only does the field property coincide perfectly with the environmental characteristics of the binding pocket but also indication for some further structural modification of indole-2-carboxamide compounds could be found. The colored polyhedra of CoMFA and CoMSIA located in the cavity of the binding pocket are direct indexes for the

kinds and magnitude of the substituents in the process of indole-2-carboxamide derivatives synthesis.

4. Conclusions

We have not only predicted the binding conformations of indole-2-carboxamide derivatives against HLGPa, but also obtained the reasonable prediction of the binding free energies employing the LGA algorithm of the AutoDock 3.0 program. The modeling results provide a satisfactory explanation for the binding mechanism of indole-2-carboxamide compounds with HLGPa, and indicate that the binding free energies of these compounds calculated by LGA algorithm correlate very well with the reported inhibitory potencies against HLGPa. On the basis of the binding conformations of indole-2-carboxamide derivatives, we have developed stable and predictive 3D-QSAR models with acceptable q^2 values by undertaking CoMFA and CoMSIA techniques, and these models could be mapped back to the 3D topology of the binding site of HLGPa. This leads to a better understanding of crucial indole-2-carboxamide–HLGPa interactions and thus provides guidelines for the structural modifications of the inhibitors and a predictive model for scoring novel synthetic candidates.

It is essential to understand protein–ligand interactions for designing novel synthetic candidates, however, those interactions are difficult to describe. Structure-based design is focused on the elucidation of enzyme–substrate interactions but does not always lead to predictive models. On the other hand, 3D-QSAR models do not necessarily reflect topological features of the protein structure. These models are generally constructed using alignment rules, which are not always consistent with the characteristics of the binding conformations. In this study, these two approaches were successfully combined; the complex 3D model of indole-2-carboxamide compounds with HLGPa was obtained by AutoDock 3.0 and predictive 3D-QSAR models were derived from the alignment conformations extracted directly from the 3D models of the inhibitor–protein complex. The predictive ability testing for the 3D-QSAR models has validated their reliability, so the application of these models for quantitative prediction of inhibitory potencies against HLGPa is possible within a structurally limited range. Therefore, the CoMFA and CoMSIA models are expected to be fast and convenient tools to design new inhibitors with higher inhibitory activities against HLGPa.

Acknowledgements

We thank Prof. Arthur J. Olson for his kindness in offering us the AutoDock 3.0.3 program. We gratefully acknowledge financial support from National Natural Science Foundation of China (Grants 20102007, 29725203, and 20072042), the State Key Program of Basic Research of China (Grant 2002CB512802), the 863 Hi-Tech Program of China (Grants 2002AA233061, 2001AA235051, and 2001AA235041), and the Key Program of New Drug Research and Development from Chinese Academy of Sciences.

References and notes

1. DeFronzo, R. A. *Diabetes* **1988**, *37*, 667.
2. Taylor, S. I. *Cell* **1999**, *97*, 9.
3. DeFronzo, R. A.; Bonadonna, R. C.; Ferrannini, E. *Diabetes Care* **1992**, *15*, 318.
4. Kenny, S. J.; Aubert, R. E.; Geiss, L. S. In *Diabetes in America*, 2nd ed.; Harris, M., Ed.; NIH Publication 95-1468; National Institutes of Health: Bethesda, MD, 1995; pp 47–67.
5. Moller, D. E. *Nature* **2001**, *414*, 821.
6. Yki-Jarvinen, H. *Diab. Nutr. Metab.* **1994**, *7*, 109.
7. Barrett, E. J.; Liu, Z. *Baillieres Clin. Endocrinol. Metab.* **1993**, *7*, 875.
8. Consoli, A. *Diabetes Care* **1992**, *15*, 430.
9. Landau, B. R.; Wahren, J.; Chandramouli, V.; Schumann, W. C.; Ekberg, K.; Kalhan, S. C. *J. Clin. Invest.* **1996**, *98*, 378.
10. Hellerstein, M. K.; Neese, R. A.; Linfoot, P.; Christiansen, M.; Turner, S.; Letscher, A. *J. Clin. Invest.* **1997**, *100*, 1305.
11. Martin, W. H.; Hoover, D. J.; Armento, S. J.; Stock, I. A.; McPherson, R. K.; Danley, D. E.; Stevenson, R. W.; Barrett, E. J.; Treadway, J. L. *Proc. Natl. Acad. Sci. U.S.A.* **1998**, *95*, 1776.
12. Martin, J. L.; Veluraja, K.; Ross, K.; Johnson, L. N.; Fleet, G. W. J.; Ramsden, N. G.; Bruce, I.; Orchard, M. G.; Oikonomakos, N. G.; Papageorgiou, A. C. *Biochemistry* **1991**, *30*, 10101.
13. Watson, K. A.; Mitchell, E. P.; Johnson, L. N.; Son, J. C.; Bichard, C. J. F.; Orchard, M. G.; Fleet, G. W. J.; Oikonomakos, N. G.; Leonidas, D. D.; Kontou, M. *Biochemistry* **1994**, *33*, 5745.
14. Watson, K. A.; Mitchell, E. P.; Johnson, L. N.; Cruciani, G.; Son, J. C.; Bichard, C. J. F.; Fleet, G. W. J.; Oikonomakos, N. G.; Kontou, M.; Zographos, S. E. *Acta Crystallogr.* **1995**, *D51*, 458.
15. Gregoriou, M.; Noble, M. E. M.; Watson, K. A.; Carman, E. F.; Krulle, T. M.; Fuente, C.; Fleet, G. W. J.; Oikonomakos, N. G.; Johnson, L. N. *Protein Sci.* **1998**, *7*, 915.
16. Oikonomakos, N. G.; Kontou, M.; Zographos, S. E.; Watson, K. A.; Johnson, L. N.; Bichard, C. J. F.; Fleet, G. W. J.; Acharya, K. R. *Protein Sci.* **1995**, *4*, 2469.
17. Newgard, C. B.; Hwang, P. K.; Fletterick, R. J. *Crit. Rev. Biochem. Mol. Biol.* **1989**, *24*, 69.
18. De la Fuente, C.; Krulle, T. M.; Watson, K. A.; Gregoriou, M.; Johnson, L. N.; Tsitsanou, K. E.; Zographos, S. E.; Oikonomakos, N. G.; Fleet, G. W. J. *Synlett* **1997**, 485.
19. Kasvinsky, P. J.; Shechosky, S.; Fletterick, R. J. *J. Biol. Chem.* **1978**, *253*, 9102.
20. Krulle, T. M.; Watson, K. A.; Gregoriou, M.; Johnson, L. N.; Crook, S.; Watkin, D. J.; Griffiths, R. C.; Nash, R. J.; Tsitsanou, K. E.; Zographos, S. E.; Oikonomakos, N. G.; Fleet, G. W. J. *Tetrahedron Lett.* **1995**, *36*, 8291.
21. Mitchell, E. P.; Withers, S. G.; Ermert, P.; Vasella, A. T.; Garman, E. F.; Oikonomakos, N. G.; Johnson, L. N. *Biochemistry* **1996**, *35*, 7341.
22. Zographos, S. E.; Oikonomakos, N. G.; Tsitsanou, K. E.; Leonidas, D. D.; Chrysina, E. D.; Skamnaki, V. T.; Bischoff, H.; Goldman, S.; Watson, K. A.; Johnson, L. N. *Structure* **1997**, *5*, 1413.

23. Bichard, C. J. F.; Mitchell, E. P.; Wormald, M. R.; Watson, K. A.; Johnson, L. N.; Zographos, S. E.; Koutra, D. D.; Oikonomakos, N. G.; Fleet, G. W. J. *Tetrahedron Lett.* **1995**, *36*, 2145.
24. Oikonomakos, N. G.; Tsitsanou, K. E.; Zographos, S. E.; Skamnaki, V. T.; Goldman, S.; Bischoff, H. *Protein Sci.* **1999**, *8*, 1930.
25. Oikonomakos, N. G.; Schnier, J. B.; Zographost, S. E.; Skamnaki, V. T.; Tsitsanou, K. E.; Johnson, L. N. *J. Biol. Chem.* **2000**, *275*, 34566.
26. Oikonomakos, N. G.; Skamnaki, V. T.; Tsitsanou, K. E.; Gavalas, N. G.; Johnson, L. N. *Structure* **2000**, *8*, 575.
27. Ekstrom, J. L.; Pauly, T. A.; Carty, M. D.; Soeller, W. C.; Culp, J.; Danley, D. E.; Hoover, D. J.; Treadway, J. L.; Gibbs, E. M.; Fletterick, R. J.; Day, Y. S. N.; Myszka, D. G.; Rath, V. L. *Chem. Biol.* **2002**, *9*, 915.
28. Oikonomakos, N. G.; Zographos, S. E.; Skamnaki, V. T.; Archontis, G. *Bioorg. Med. Chem.* **2002**, *10*, 1313.
29. Hoover, D. J.; Lefkowitz-Snow, S.; Burgess-Henry, J. L.; Martin, W. H.; Armento, S. J.; Stock, I. A.; McPherson, P. K.; Genereux, P. E.; Gibbs, E. M.; Treadway, J. L. *J. Med. Chem.* **1998**, *41*, 2934.
30. Rath, V. L.; Ammirati, M.; Danley, D. E.; Ekstrom, J. L.; Gibbs, E. M.; Hynes, T. R.; Mathiowetz, A. M.; McPherson, R. K.; Olson, T. V.; Treadway, J. L.; Hoover, D. J. *Chem. Biol.* **2000**, *7*, 677.
31. Tracey, W. R.; Treadway, J. L.; Magee, W. P.; Sutt, J. C.; McPherson, R. K.; Levy, C. B.; Wilder, D. E.; Yu, L. J.; Chen, Y.; Shanker, R. M.; Mutchler, A. K.; Smith, A. H.; Flynn, D. M.; Knight, D. R. *Am. J. Physiol. Heart Circ. Physiol.* **2004**, *286*, 1177.
32. Oikonomakos, N. G.; Chrysina, E. D.; Kosmopoulou, M. N.; Leonida, D. D. *Biochim. Biophys. Acta* **2003**, *1647*, 325.
33. Cramer, M.; Cramer, R. D., III; Jones, D. M. *J. Am. Chem. Soc.* **1988**, *110*, 5959.
34. Klebe, G.; Abraham, U.; Mietzner, T. *J. Med. Chem.* **1994**, *37*, 4130.
35. Sybyl, Version 6.8; Tripos Associates: St. Louis, MO, 2000.
36. Weiner, S. J.; Kollman, P. A.; Case, D. A.; Singh, C.; Ghio, G.; Alagona, S.; Profeta, P.; Weiner, P. *J. Am. Chem. Soc.* **1984**, *106*, 765. Details of the implementation are given in Sybyl 6.5 Theory Manual; Tripos: St. Louis, MO, 1998; p 441.
37. Halgren, T. *J. Am. Chem. Soc.* **1990**, *112*, 4710.
38. Huang, X.; Liu, T.; Gu, J.; Luo, X.; Ji, R.; Cao, Y.; Xue, H.; Wong, J. T.; Wong, B. L.; Pei, G.; Jiang, H.; Chen, K. *J. Med. Chem.* **2001**, *44*, 1883.
39. Huang, X.; Xu, L.; Luo, X.; Fan, K.; Ji, R.; Pei, G.; Chen, K.; Jiang, H. *J. Med. Chem.* **2002**, *45*, 333.
40. Liu, H.; Huang, X.; Shen, J.; Luo, X.; Li, M.; Xiong, B.; Chen, G.; Shen, J.; Yang, Y.; Jiang, H.; Chen, K. *J. Med. Chem.* **2002**, *45*, 4816.
41. Morris, G. M.; Goodsell, D. S.; Huey, R.; Hart, W. E.; Halliday, S.; Belew, R.; Olson, A. J. AutoDock Version 3.0.3. The Scripps Research Institute, Molecular Graphics Laboratory, Department of Molecular Biology, 1999.
42. Morris, G. M.; Goodsell, D. S.; Halliday, R. S.; Huey, R.; Hart, W. E.; Belew, R. K.; Olson, A. J. *J. Comput. Chem.* **1998**, *19*, 1639.
43. Solis, F. J.; Wets, R. J. B. *Maths. Pera. Res.* **1981**, *6*, 19.
44. Morris, G. M.; Goodsell, D. S.; Huey, R.; Olson, A. J. *J. Comput.-Aided Mol. Des.* **1996**, *10*, 293.
45. Purcel, W. P.; Singer, J. A. *J. Chem. Eng. Data* **1967**, *12*, 235. Details of the implementation are given in Sybyl 6.5 Theory Manual; Tripos: St. Louis, MO, 1998; p 69.
46. Ghose, A. K.; Viswanadhan, V. N.; Wendoloski, J. J. *J. Comb. Chem.* **1999**, *1*, 55.